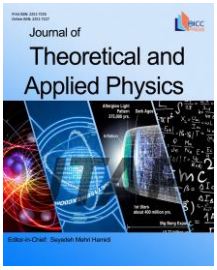

J. Theor. Appl. Phys., 2026; 20(2): 141-151

Journal of Theoretical and Applied Physics (JTAP)

https://doi.org/10.57647/jtap.2026.2002.14

Research Article

Pressure–Volume Response in Nanomaterials: Contrasting Graphenic Sheets, Oxide Ceramics, and Transition Metal Architectures

Tajamul Islam[1], A.K Srivastava[1], Mudasir Mir[2], Santosh Chackrabarti[3*], R.A. Zargar[4]

[1]*Department of Physics, Lovely Professional University, 144411, Phagwara, Punjab*
[2]*Department of Physics, Government Degree College, Shopian(J&K)*
[3]*Centre for nanoscience and nanotechnology, 110025, Jamia Millia Islamia, New Delhi*
[4]*Department of Physics, Guru Nanak University, 501506, Ibrahimpatnam, Telangana*

***Corresponding author:** dhrub.phy@gmail.com

Article History:

Received:
14 October 2025

Revised:
21 November 2025

Accepted:
17 December 2025

Published Online:
05 February 2026

Published in Issue:
30 April 2026

Abstract

This investigation presents a comprehensive theoretical examination of pressure-induced volumetric compression characteristics in five structurally diverse nanomaterials: graphite, aluminium oxide (Al_2O_3), single-walled carbon nanotubes (SWCNTs), nano-epsilon-phase iron (nano-ε-Fe), and nano-nickel (nano-Ni), representing carbon allotropes, ceramic oxides, and transition metal systems. Four established equations of state (Tait, Murnaghan, Kholiya and Chandra, and Shanker) were employed using experimentally derived bulk modulus values and their pressure derivatives from literature to model relative volumetric changes under applied pressure up to 16 GPa. The analysis reveals material-specific compressibility behaviours dictated by bonding characteristics, atomic configuration, and dimensionality. Al_2O_3 demonstrates the highest incompressibility among studied materials due to its strong ionic-covalent bonding, while SWCNTs exhibit pronounced nonlinear compression attributed to structural instabilities under confinement. Nano-Ni and nano-ε-Fe show intermediate compressibility with enhanced sensitivity due to nanoscale effects including surface energy influences and modified coordination environments. The study validates the applicability of classical equations of state for predicting nanoscale mechanical responses and provides critical insights for material selection in nanodevice design for biomedical, energy, and high-pressure applications.

Keywords: Nanomaterial, equation of state, compression, volume, pressure

Cite this article: Islam, T., Srivastava, A.K., Mir, M., Chackrabarti, S. & Zargar, R.A., (2026). Pressure–Volume Response in Nanomaterials: Contrasting Graphenic Sheets, Oxide Ceramics, and Transition Metal Architectures. *J. Theor. Appl. Phys.,* 20(2), 141-151 https://doi.org/10.57647/jtap.2026.2002.14

1. Introduction

Nanomaterials have surfaced as pivotal agents in the realm of materials science, presenting distinctive properties that stem from their elevated surface area-to-volume ratios and quantum phenomena [1–3]. These nanoscale materials demonstrate unique physical and chemical characteristics when juxtaposed with their bulk counterparts, exhibiting

properties that are markedly responsive to various external factors, including temperature, pressure, and ambient conditions [4–6]. Notably, pressure assumes a crucial role in the modulation of interatomic separations, phase stability, and mechanical responses, consequently affecting the functional attributes of nanomaterials [7–11].

Among the extensive variety of nanomaterials, carbon-based entities such as single-walled carbon nanotubes (SWCNTs) and graphite have undergone thorough investigation. SWCNTs are distinguished for their remarkable electrical conductivity, tensile strength, and thermal stability, rendering them appropriate for utilization in electronics, energy storage, and biomedical applications [12–14]. Graphite, which consists of layered graphene sheets, functions as a fundamental component across various sectors owing to its outstanding electrical conductivity, elevated thermal resistance, and structural durability, particularly within energy storage frameworks like lithium-ion batteries [15–17]. In addition to carbon-derived nanomaterials, metal oxides and metallic nanoparticles have attracted considerable scholarly interest. Among metal oxides, Aluminum oxide (Al_2O_3) nanoparticles display exceptional hardness, thermal stability, and dielectric characteristics, which enhance their applicability in microelectronics, protective coatings, and ceramic composites [18,19]. Particularly, γ- Al_2O_3 nanoparticles produced under high-pressure conditions exhibit improved structural attributes, which are essential for applications necessitating mechanical robustness [20]. Similarly, transition metal-based nanomaterial like Epsilon-phase iron oxide (ε-Fe_2O_3) nanoparticles exhibit distinctive magnetic characteristics, encompassing an exceptionally high coercive field and pronounced ferromagnetic resonance, which are of paramount importance for applications in high-density magnetic storage and spintronic devices [21-23]. Empirical investigations have indicated that ε-Fe_2O_3 sustains structural integrity under pressures reaching 27 GPa; beyond this threshold, a volumetric collapse transpires, signifying a phase transition that may be harnessed for pressure-sensitive technologies [24]. Likewise, Nickel nanoparticles (nano Ni) are distinguished by their remarkable catalytic performance, magnetic attributes, and mechanical durability. Contemporary studies have revealed that single-crystalline nickel nanoparticles display ultrahigh compressive strength, attaining levels up to 34 GPa, a feat that is unparalleled among metallic substances and approaches the theoretical strength limits of nickel [24,25].

These exceptional properties render nano Ni a highly promising candidate for applications in catalysis, energy conversion, and as reinforcement agents within composite materials.

Grasping the dynamics of these nanomaterials under elevated pressure conditions is imperative for their incorporation into sophisticated technological applications. Modifications induced by pressure can result in phase transitions, modifications of electronic configurations, and enhanced mechanical characteristics, which are vital for the advancement of next-generation materials [26-39]. The equation of state (EOS), particularly the relationship between volume compression and pressure, functions as a fundamental instrument for investigating the mechanical durability and structural integrity of nanomaterials [7–9].

In this research, we provide a comparative examination of five representative nanomaterials single-walled carbon nanotubes (SWCNTs), graphite, aluminum oxide (Al_2O_3), nano ε-iron, and nano nickel in high-pressure environments.

By employing the EOS framework, we explore their volume compressibility characteristics and evaluate structural integrity over a spectrum of pressures. The results are corroborated against experimental standards and analyzed within the framework of their prospective applications in high-stakes biomedical and technological fields.

2. Methods of analysis

The analytical framework employed in this study is based on equations of state (EOS), which describe the relationship between thermodynamic variables including pressure (P), volume (V), and temperature (T) for any material system [40-43].

These equations enable prediction of material behavior under various pressure, volume, and temperature conditions for both pure components and multicomponent mixtures [44].

EOS relationships are instrumental in describing material stability by correlating different parameters such as entropy, temperature, pressure, and volume, thereby reflecting atomic structure, chemical bonding, and material stability [45-47].

2.1. Equation of state models

Four established equations of state were utilized to determine pressure-dependent volume compression and bulk modulus behavior: the Tait equation [47, 48], Murnaghan EOS [49, 50], Kholiya and Chandra EOS [51], and Shanker's EOS [52, 53].

The comparative analysis using multiple models provides insight into model-dependent variations and helps identify the most suitable approach for each material type. Each model has specific applicability and underlying assumptions:

10.57647/jtap.2026.2002.14

2.1.1. *Tait equation of state*

The Tait equation, originally developed for liquid compression behavior, has been successfully extended to solid materials. The modified Tait equation (Usual Tait Equation - UTE) is expressed as:

$$\frac{V}{V_0} = \left[1 + \left(\frac{B_0' P}{B_0}\right)\right]^{-1/B_0'} \quad (1)$$

where V_0 is the reference volume at zero pressure, B_0 is the bulk modulus at zero pressure, B_0' is the pressure derivative of the bulk modulus, and P is the applied pressure. The isothermal bulk modulus K(P) derived from this equation is:

$$K(P) = B_0[1 + \left(\frac{B_0' P}{B_0}\right)] \quad (2)$$

2.1.2. *Murnaghan equation of state*

The Murnaghan EOS is widely used for describing pressure-volume relationships of materials under static high compression, particularly suitable for materials with relatively uniform compression behavior:

$$P = \frac{B_0}{B_0'}\left[\exp\left\{-B_0' \ln\left(\frac{V}{V_0}\right)\right\} - 1\right] \quad (3)$$

This equation assumes that the bulk modulus varies linearly with pressure and is most accurate for moderate pressure ranges.

2.1.3. *Kholiya and chandra equation of state*

This equation was specifically developed for nanomaterials, accounting for size-dependent effects and surface energy contributions:

$$P = \frac{B_0}{2}\left[(B_0' - 3) - 2(B_0' - 2)\left(\frac{V}{V_0}\right)^{-1} + (B_0' - 1)\left(\frac{V}{V_0}\right)^{-2}\right] \quad (4)$$

This model is particularly effective for materials where surface effects and nanoscale phenomena significantly influence mechanical properties.

2.1.4. *Shanker's equation of state*

Shanker's equation incorporates higher-order elasticity terms and is suitable for materials exhibiting nonlinear compression behavior:

$$P = B_0\left[\left(1 - \frac{V}{V_0}\right) + \left(B_0' + \frac{1}{2}\right)\left(1 - \left(\frac{V}{V_0}\right)^2\right)\right] \quad (5)$$

This model is effective for capturing complex mechanical responses, particularly in materials with significant anharmonicity. The selection of these four EOS models was based on their complementary strengths and applicability ranges. Tait equation is excellent for general compression behavior with good mathematical stability. Murnaghan equation is well-established for crystalline materials under moderate pressures. Kholiya and Chandra equation is specifically designed for nanomaterials with surface effects. Shanker's equation captures nonlinear behavior and anharmonic effects. While, there are certain limitations with these models. Tait and Murnaghan equations may underestimate surface effects in nanomaterials. Kholiya and Chandra equation requires careful parameter selection for optimal accuracy. Shanker's equation may overpredict compression at extreme pressures. All models assume isothermal conditions and may not account for dynamic loading effects. It is worth mentioning here that all four EOS models employed in this study assume isotropic or quasi-isotropic material behavior, utilizing scalar bulk modulus and its pressure derivative as input parameters. For materials with significant mechanical anisotropy (such as SWCNTs and graphite), the bulk modulus represents an effective volumetric response under hydrostatic compression, predominantly reflecting deformation along the most compliant crystallographic direction or averaged over multiple grain orientations in polycrystalline samples. The bulk modulus (B_0) and pressure derivative (B_0') values used as input parameters (Table 1) were obtained from experimental measurements on nanoscale samples, ensuring that our theoretical predictions reflect the actual mechanical behavior of nanostructured materials including inherent nanoscale effects such as grain boundaries, surface energy contributions, and size-dependent elastic moduli.

3. Results and discussion

3.1. Input parameters

The bulk modulus (B_0) and its pressure derivative (B_0') values used in this study were obtained from established experimental literature and are presented in Table 1.

Table 1. Input data of SWCNTs, Graphite, Al_2O_3, Nano-ε-Fe, Nano Ni

Compounds	B_0 (GPa)	B_0'(GPa)	Source
SWCNTs	37	11	Ref [13-16]
Graphite	33.8	8.9	Ref [17,32,33]
Al_2O_3	248	3.2	Ref [18-20]
Nano-ε-Fe	179	3.6	Ref [21-23]
Nano Ni	185.4	4	Ref [24,25]

These parameters are critical for accurate EOS calculations and were selected based on their reliability and consistency across multiple experimental studies.

3.2. Graphite compression analysis

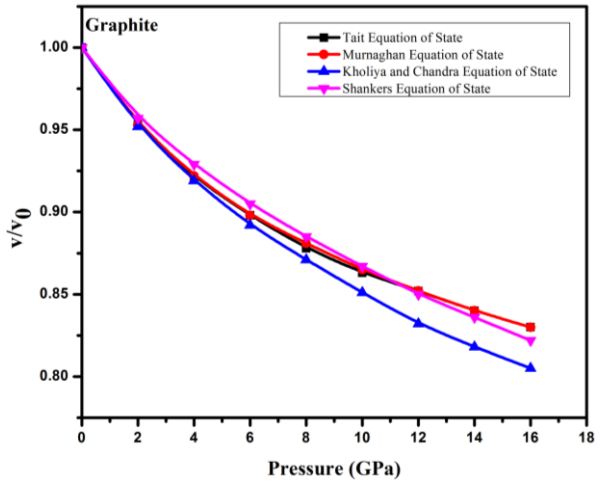

Figure 1. Variation compression of volume of graphite with respect to the Pressure

Table 2. Data regarding compression of Graphite material by different EOS

Pressure (GPa)	Tait Model	Murnaghan Model	Kholiya and Chandra Model	Shankers Model
	V/V_0	V/V_0	V/V_0	V/V_0
0	1	1	1	1
2	0.953	0.953	0.952	0.957
4	0.921	0.922	0.919	0.929
6	0.898	0.898	0.892	0.905
8	0.878	0.881	0.871	0.885
10	0.863	0.865	0.851	0.867
12	0.852	0.852	0.832	0.85
14	0.84	0.84	0.818	0.836
16	0.83	0.83	0.805	0.822

The compression behavior of Graphite at various pressures (in GPa) with the help of different EOS is illustrated in Table 2 and Figure 1. Graphite demonstrates a continuous reduction in relative volume (V/V_o) in response to increasing pressure. This phenomenon is fundamentally linked to the characteristics of graphite's anisotropic layered architecture, wherein the weak van der Waals interactions between graphene layers facilitate comparatively easier compaction along the c-axis. All four equations of state (EOS) models exhibit a downward trend, with the Kholiya and Chandra model predicting the most pronounced loss of volume, thereby indicating an increased sensitivity to variations in pressure. In contrast, the Tait and Murnaghan models display consistent and moderate compressibility, while the Shanker model suggests a marginally less steep decline. This observed behavior underscores the significance of interlayer interactions in graphite's structural response to applied pressure. As compression intensifies, the interlayer spacing diminishes, resulting in a reduction in volume until a critical threshold is reached, beyond which additional compression necessitates elevated energy levels due to electron cloud repulsion. This divergence among EOS arises because Tait and Murnaghan assume quasi-linear compressibility, while Kohliya–Chandra and Shanker include nonlinear and nanoscale corrections, leading to sharper predicted volume loss.

3.3. Al_2O_3 compression analysis

Al_2O_3 exhibits the highest incompressibility among the studied nanomaterials (though not globally, as diamond and other ultrahard materials show lower compressibility), confirming the strength of its ionic-covalent bonding framework. As shown in Figure 2, minimal volume contraction occurs even at elevated pressures, with slightly more pronounced changes observed in the Shanker model at higher pressures. This behavior reflects Al_2O_3's dense atomic packing and strong directional Al-O bonds that resist compressive forces. At the nanoscale, size-dependent surface phenomena may slightly reduce the rigidity typically associated with bulk Al_2O_3, explaining the marginal increase in compressibility observed in some models. The convergence of EOS models at lower pressures indicates consistent elastic behavior, while divergence at higher pressures suggests the emergence of nanoscale grain boundary effects. These findings align with the known mechanical properties of ceramic oxides, where strong ionic-covalent bonding provides exceptional resistance to compression.

The material's behavior validates its suitability for applications requiring dimensional stability under mechanical loading, particularly in demanding biomedical and electronic environments. It is important to note that the bulk modulus value employed in our calculations ($B_0 = 248$ GPa) was derived from experimental measurements on nanocrystalline Al_2O_3 samples with grain sizes typically ranging from 20-80 nm [18-20], rather than single-crystal data. Consequently, our theoretical predictions inherently incorporate grain boundary effects through the experimentally determined elastic parameters. High-pressure transmission electron microscopy studies have demonstrated that grain boundaries in nano-Al_2O_3 exhibit enhanced compressibility (approximately 10-20% greater than grain interiors) due to reduced atomic coordination and increased free volume [59]. However, for grain sizes exceeding 20 nm, grain boundary volume fractions remain below 10%, meaning that the bulk mechanical response is dominated by grain interior elastic properties [60].

Table 3. Data regarding compression of Al_2O_3 material by different EOS

Pressure (GPa)	Tait Model	Murnaghan Model	Kholiya and Chandra Model	Shankers Model
	V/V_0	V/V_0	V/V_0	V/V_0
0	1	1	1	1
2	0.992	0.992	0.992	0.998
4	0.984	0.984	0.984	0.996
6	0.977	0.976	0.976	0.995
8	0.969	0.969	0.969	0.993
10	0.962	0.962	0.962	0.992
12	0.956	0.956	0.955	0.99
14	0.949	0.949	0.949	0.988
16	0.943	0.943	0.942	0.987

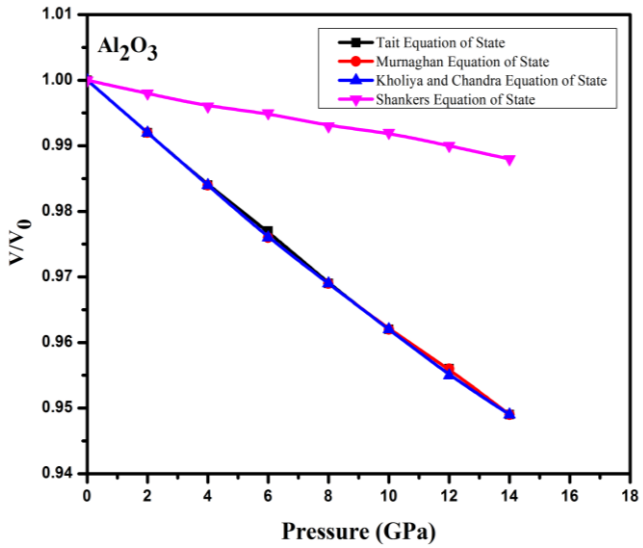

Figure 2. Variation compression of volume of Al_2O_3 with respect to the Pressure

The excellent agreement among all four EOS models for Al_2O_3 (inter-model variation <1% at 16 GPa) suggests that grain boundary contributions, while present, do not introduce significant nonlinear behavior in the studied pressure regime.

At higher pressures (>10 GPa), grain boundary densification further reduces their mechanical influence, resulting in the predominantly uniform elastic compression behavior observed in our calculations.

3.4. SWCNT compression analysis

The compression results for SWCNTs presented in Figure 3 reveal significant volume reduction with increasing pressure, particularly pronounced beyond 10 GPa. The Kholiya and Chandra model and Shanker model predict the most substantial compression, suggesting potential structural modifications such as radial collapse or wall flattening phenomena commonly observed in SWCNTs under axial loading. SWCNTs exhibit pronounced nonlinear mechanical response characteristics due to their unique one-dimensional geometry and high aspect ratio. The structural instability arises from the hollow cylindrical structure's susceptibility to radial deformation under pressure. As pressure increases, the nanotube walls experience increasing stress concentration, leading to progressive deformation that manifests as rapid volume reduction.

The divergence among EOS models at high pressures indicates the onset of complex deformation mechanisms. Under extreme confinement, SWCNTs may undergo irreversible structural changes including wall buckling, cross-sectional flattening, or even complete collapse, which explains the limiting behavior observed in the pressure-volume curves. SWCNTs often undergo radial collapse and ovalization under pressures beyond 10 GPa, as reported in high-pressure Raman and XRD studies [15–17, 29–31].

The pronounced nonlinear compression behavior predicted by our models, particularly evident beyond 10 GPa, is consistent with experimental observations from high-pressure studies. Synchrotron XRD investigations by Sharma et al. [54] documented cross-sectional distortion in SWCNTs under hydrostatic pressure exceeding 8 GPa, while Raman spectroscopy studies by Venkateswaran et al. [55] reported radial breathing mode softening indicative of structural deformation at similar pressure ranges. The structural instability manifests primarily as radial collapse (also termed radial buckling or ovalization), wherein the circular cross-section transforms into an elliptical or polygonal configuration, eventually leading to wall-wall contact at critical pressures [56, 57]. This radial collapse mechanism, rather than axial buckling, is the dominant deformation mode under hydrostatic compression conditions, with critical collapse pressure scaling inversely with nanotube diameter [58]. The diameter-dependent nature of this instability, combined with diameter distribution in SWCNT samples, contributes to the observed nonlinear compression characteristics and explains the model-dependent variations at higher pressures where structural transformations become increasingly significant. It must be emphasized that SWCNTs exhibit highly anisotropic mechanical properties, with radial and axial bulk moduli differing by factors of 20-50 [61, 62]. The radial bulk modulus (K_{radial} ≈ 15-40 GPa) reflects the compressibility of van der Waals gaps between tubes and the deformability of the tube cross-section, while the axial bulk modulus (K_{axial} ≈ 600-900 GPa) represents the extreme stiffness of covalent C-C bonds along the tube axis [63]. Our study employs an effective isotropic bulk modulus (B_0 = 37 GPa) obtained from hydrostatic compression experiments, which predominantly reflects radial-dominated volumetric response. This treatment is appropriate for the following

reasons: (1) under hydrostatic pressure conditions, volume change is dominated by radial compression rather than axial compression due to the extreme stiffness anisotropy; (2) in SWCNT bundles with random tube orientations or polycrystalline-like arrangements, macroscopic mechanical response approaches quasi-isotropic behavior despite individual tube anisotropy; (3) the experimentally determined bulk modulus inherently represents volume-averaged response under hydrostatic conditions; and (4) the four EOS models employed in this study were formulated for isotropic or quasi-isotropic materials using scalar bulk modulus parameters. We acknowledge that this isotropic treatment represents a limitation for applications involving uniaxial loading or single-tube mechanical analysis, where fully anisotropic continuum models or atomistic simulations would be necessary [64, 65]. Future studies incorporating direction-dependent elastic constants within anisotropic EOS frameworks would provide more complete descriptions of SWCNT compression behavior under non-hydrostatic conditions.

Table 4. Data regarding compression of SWCNT's material by different EOS

Pressure (GPa)	Tait Model	Murnaghan Model	Kholiya and Chandra Model	Shanker s Model
	V/V_0	V/V_0	V/V_0	V/V_0
0	1	1	1	1
2	0.959	0.958	0.957	0.966
4	0.931	0.931	0.92	0.932
6	0.911	0.911	0.88	0.898
8	0.895	0.895	0.85	0.863
10	0.884	0.882	0.81	0.827
12	0.867	0.871	0.78	0.791
14	0.858	0.861	0.734	0.755
16	0.849	0.852	0.71	0.718

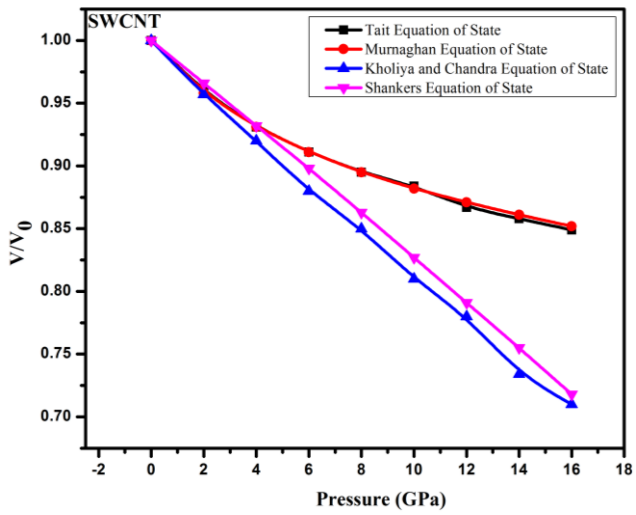

Figure 3. Variation compression of volume of SWCNT's with respect to the Pressure

3.5. Nano-Ni compression analysis

Nano-Ni exhibits moderate compressibility across all EOS models, with V/V_0 values consistently decreasing with pressure increase. The Shanker model shows the most distinct variation, suggesting enhanced elastic deformation capacity attributed to surface energy effects and reduced atomic coordination in nanoparticle configurations.

As a face-centered cubic (FCC) transition metal, nickel is recognized for its ductility in bulk form. At the nanoscale, this ductility is enhanced by increased grain boundary mobility and surface atom contribution, leading to greater pressure sensitivity.

Recent experimental studies on nickel nanoparticles have demonstrated that reduced coordination numbers at surfaces and interfaces contribute to modified mechanical properties compared to bulk materials.

The enhanced compressibility in nano-Ni can be attributed to the high surface-to-volume ratio characteristic of nanoparticles.

Table 5. Data regarding compression of Nano-Ni material by different EOS

Pressure (GPa)	Tait Model	Murnagha n Model	Kholiya and Chandra Model	Shankers Model
	V/V_0	V/V_0	V/V_0	V/V_0
0	1	1	1	1
2	0.989	0.989	0.988	0.996
4	0.979	0.979	0.979	0.99
6	0.969	0.97	0.97	0.989
8	0.96	0.96	0.96	0.98
10	0.951	0.952	0.952	0.978
12	0.942	0.944	0.943	0.971
14	0.934	0.936	0.935	0.967
16	0.925	0.928	0.928	0.962

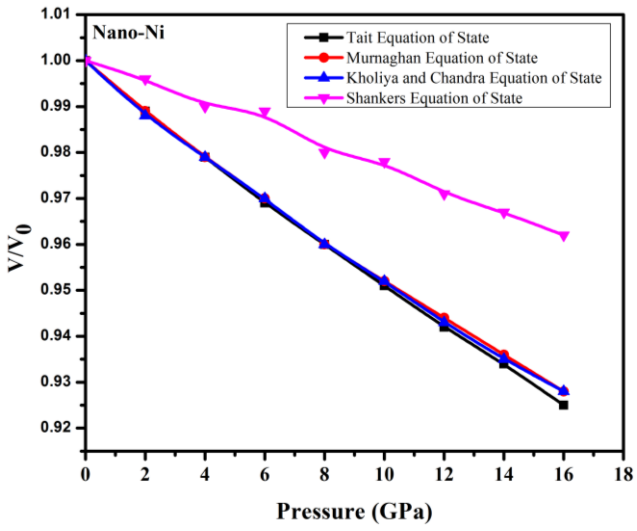

Figure 4. Variation compression of volume of Nano-Ni with respect to the Pressure

Surface atoms, having lower coordination numbers, exhibit different bonding environments that can accommodate deformation more readily than bulk atoms. This nanoscale effect becomes particularly prominent under applied stress, contributing to the material's adaptability under mechanical loading. Prior studies [24,25] confirm enhanced ductility in nano-Ni due to grain boundary mobility and surface energy effects.

3.6. Nano-ε-Fe compression analysis

Nano-ε-Fe exhibits compression behavior similar to nano-Ni but with slightly reduced volume loss under pressure, as shown in Table 6 and Figure 5. This characteristic can be attributed to the denser atomic packing inherent in the hexagonal close-packed (HCP) structure compared to face-centered cubic (FCC) arrangements. The near-overlapping results among all EOS models suggest high structural stability and isotropy in compression response.

Table 6. Data regarding compression of Nano-ε-Fe material by different EOS

Pressure (GPa)	Tait Equation	Murnaghan Equation	Kholiya and Chandra Equation	Shankers Equation
	V/V_0	V/V_0	V/V_0	V/V_0
0	1	1	1	1
2	0.989	0.989	0.989	0.991
4	0.978	0.978	0.978	0.98
6	0.968	0.968	0.968	0.971
8	0.959	0.959	0.959	0.961
10	0.95	0.95	0.95	0.952
12	0.941	0.941	0.941	0.943
14	0.933	0.933	0.933	0.936
16	0.925	0.925	0.925	0.927

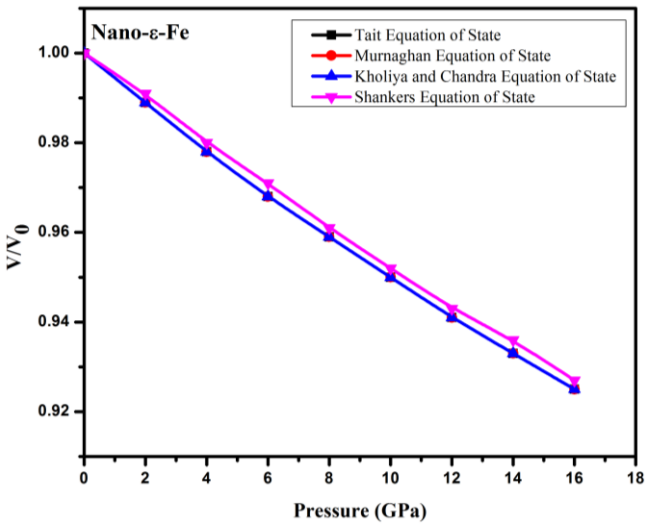

Figure 5. Variation compression of volume of Nano-ε-Fe with respect to the Pressure

The ε-phase demonstrates exceptional incompressibility under elevated pressure conditions, evidenced by the gradual volume reduction trends observed in the initial pressure stages. As pressure increases, interatomic distances decrease; however, the strong metallic bonding in ε-Fe provides substantial resistance to volumetric collapse. This intrinsic stability is crucial for high-pressure applications including planetary core simulations and medical instrument miniaturization, where maintaining mechanical integrity under extreme conditions is essential. The material's behavior suggests suitability for applications requiring structural stability under variable pressure conditions. Literature reports [21–23] validate the high-pressure stability of ε-Fe, linking its resistance to volumetric collapse with dense atomic packing.

3.7. Comparative analysis and model performance

The comparative analysis across all five nanomaterials reveals distinct material-specific responses and systematic model-dependent variations that provide crucial insights into the applicability of different equations of state for nanoscale systems. The Tait and Murnaghan models demonstrate excellent agreement for most materials, particularly showing consistent predictions for Al_2O_3 and nano-ε-Fe, which can be attributed to these materials' relatively uniform compression behavior and strong interatomic bonding that aligns well with the linear bulk modulus assumptions inherent in these classical formulations. In contrast, the Kholiya and Chandra model consistently predicts more pronounced compression across all materials, especially for carbon-based structures (SWCNTs and graphite), reflecting its specific design to account for nanoscale surface effects and size-dependent phenomena that become increasingly significant in low-dimensional materials. Shanker's model captures intermediate compression behavior with particularly good representation of nanoscale effects in metallic nanoparticles, where its incorporation of higher-order elasticity terms effectively describes the enhanced deformation capacity arising from surface energy influences and reduced atomic coordination. Material-specific trends reveal that Al_2O_3 demonstrates the highest incompressibility with minimal inter-model variation (less than 1% difference at 16 GPa), validating the robustness of all EOS approaches for highly incompressible ceramic systems, while SWCNTs exhibit the largest model-dependent differences (up to 15% variation at 16 GPa), indicating complex deformation mechanisms including potential structural instabilities that challenge the applicability of classical continuum-based formulations. The metallic nanoparticles (nano-Ni and nano-ε-Fe)

display consistent moderate compressibility across models with systematic deviations primarily emerging in the Shanker formulation, suggesting that nanoscale metallic systems benefit from models incorporating anharmonic effects, while graphite shows intermediate compression with good inter-model correlation except at the highest pressures where interlayer interactions become increasingly nonlinear. Notably, all materials exhibit increasing model divergence at pressures exceeding 10 GPa, indicating the onset of nonlinear deformation mechanisms, potential phase transitions, or structural instabilities that are not fully captured by the linearized assumptions underlying classical EOS formulations, thereby highlighting the need for more sophisticated theoretical approaches or experimental validation when extending predictions to extreme pressure regimes in nanoscale systems.

4. Conclusion

This comparative investigation systematically examines the volumetric compression characteristics of five structurally diverse nanomaterials- SWCNTs, graphite, Al_2O_3, nano-ε-Fe, and nano-Ni- under applied pressure using four theoretical equations of state. The analysis reveals material-specific compression behaviors influenced by bonding characteristics, atomic configuration, and dimensionality effects. Al_2O_3 exhibits the highest incompressibility among studied materials due to strong ionic-covalent bonding, with minimal compression even under high pressures, validating its suitability for applications requiring dimensional stability. SWCNTs demonstrate pronounced nonlinear compression behavior attributed to structural instabilities arising from their unique one-dimensional geometry and hollow structure, showing significant model-dependent variations at higher pressures. Nano-Ni displays enhanced elastic responsiveness compared to bulk counterparts, influenced by surface energy effects and reduced atomic coordination in nanoparticle configurations. Nano-ε-Fe maintains exceptional structural stability with minimal compression variation across all EOS models, reflecting the dense atomic packing of the hexagonal close-packed structure. Graphite shows intermediate compression behavior dominated by interlayer interactions, with consistent trends across most EOS models. The study validates the predictive capability of classical equations of state for nanoscale mechanical responses while highlighting the importance of model selection based on material type and pressure range. The observed differences between EOS models at elevated pressures underscore the complexity of nanomaterial behavior under extreme conditions. These insights provide a significant framework for tailoring nanomaterials in advanced applications requiring superior mechanical performance and precision, particularly in biomedical engineering, energy systems, and miniaturized devices operating under stress. Several important limitations should be noted.

As a purely theoretical investigation, the predictions presented here would benefit from experimental validation through high-pressure XRD, Raman spectroscopy, or TEM measurements, which we recommend for future work. Likewise, the isotropic EOS framework used in this study is best suited for materials with cubic or quasi-isotropic behavior. For highly anisotropic systems such as SWCNTs and graphite, the extracted bulk modulus represents a direction-averaged or radially dominated response rather than a complete description of their tensorial mechanical properties. A fully anisotropic analysis would require direction-dependent elastic constants and tensor-based EOS models, which remain a promising avenue for future theoretical development. Also, the present models assume isothermal conditions and do not incorporate potential temperature-dependent effects or dynamic loading behavior. Despite these limitations, the comparative framework established here contributes to the rational design and selection of nanomaterials for specific high-performance applications.

Funding

There was no funding during this research tenure.

Authors Contribution

Tajamul Islam and A.K.Srivastava : Methodology and Formal Analysis ; Mudasir Mir : Software ; Santosh Chackrabarti : Conceptualization and Writing- Original Draft ; R.A.Zargar : Validation and Supervision.'

Availability of data and materials

Data will be made available upon reasonable request.

Conflict of interests

The authors declare no competing interests.

References

[1] Borisenko, V. E., & Ossicini, S. (2013). *What is what in the nanoworld: A handbook on nanoscience and nanotechnology*. John Wiley & Sons.

[2] Joachim, C. (2009). *Nanosciences: The invisible revolution*. World Scientific.

[3] Wilson, M., Kannangara, K., Smith, G., Simmons, M., & Raguse, B. (2002). *Nanotechnology: Basic science and emerging technologies*. Chapman and Hall/CRC.

[4] Minnich, A., Dresselhaus, M. S., Ren, Z. F., & Chen, G. (2009). Bulk nanostructured thermoelectric materials: Current research and future prospects. Energy &

Environmental Science, *2*(5), 466-479.

[5] Yoon, H., & Jang, J. (2009). Conducting-polymer nanomaterials for high-performance sensor applications: Issues and challenges. *Advanced Functional Materials*, *19*(10), 1567-1576.

[6] Tan, J. C., & Cheetham, A. K. (2011). Mechanical properties of hybrid inorganic-organic framework materials: Establishing fundamental structure-property relationships. *Chemical Society Reviews*, *40*(2), 1059-1080.

[7] San-Miguel, A. (2006). Nanomaterials under high-pressure. *Chemical Society Reviews*, *35*(10), 876-889.

[8] Roduner, E. (2007). *Nanoscopic materials: Size-dependent phenomena*. Royal Society of Chemistry.

[9] Ali, N., Teixeira, J. A., & Addali, A. (2018). A review on nanofluids: Fabrication, stability, and thermophysical properties. *Journal of Nanomaterials*, *2018*, 1-33.

[10] Cao, G. (2004). *Nanostructures & nanomaterials: Synthesis, properties & applications*. Imperial College Press.

[11] Guo, D., Xie, G., & Luo, J. (2013). Mechanical properties of nanoparticles: Basics and applications. *Journal of Physics D: Applied Physics*, *47*(1), 013001.

[12] Goyal, M., & Gupta, B. R. K. (2019). Study of shape, size and temperature-dependent elastic properties of nanomaterials. *Modern Physics Letters B*, *33*(26), 1950310.

[13] Wu, Q., Miao, W. S., Zhang, Y. D., Gao, H. J., & Hui, D. (2020). Mechanical properties of nanomaterials: A review. *Nanotechnology Reviews*, *9*(1), 259-273.

[14] Kiio, T. M., & Park, S. (2021). Physical properties of nanoparticles do matter. *Journal of Pharmaceutical Investigation*, *51*, 35-51.

[15] Chandrasekhar, P. (2018). Physical, Mechanical, and Thermal Properties of CNTs. In: Conducting Polymers, Fundamentals and Applications. Springer, Cham. https://doi.org/10.1007/978-3-319-69378-1_4

[16] Palit, S. (2018). Carbon nanotubes and its applications in diverse areas of science and engineering: A critical overview. In *Engineered carbon nanotubes and nanofibrous material* (pp. 1-27). Apple Academic Press.

[17] Ooi, N., Rairkar, A., & Adams, J. B. (2006). *Density functional study of graphite bulk and surface properties*. *Carbon*, *44*(2), 231-242.

[18] Ouyang, Y., Bai, L., Tian, H., Li, X., & Yuan, F. (2022). Recent progress of thermal conductive polymer composites: Al_2O_3 fillers, properties and applications. *Composites Part A: Applied Science and Manufacturing*, *152*, 106685.

[19] Koli, D. K., Agnihotri, G., & Purohit, R. (2014). A review on properties, behaviour and processing methods for Al-nano Al_2O_3 composites. *Procedia Materials Science*, *6*, 567-589.

[20] Liang, F., Wei, Y., Du, Y., Yang, F., Pang, Z., Wu, J., Jing, L., Huo, K., & Shi, G. (2025). Foamed ceramic based γ-Al_2O_3 coated catalysts with different preparation methods for ethyl nicotinate hydrogenation reaction. *Ceramics International*, *51*(2), 1574-1584.

[21] Bykova, E., Dubrovinsky, L., Dubrovinskaia, N., Bykov, M., McCammon, C., Ovsyannikov, S. V., Liermann, H.-P., Kupenko, I., Chumakov, A. I., Rüffer, R., Hanfland, M., & Prakapenka, V. (2016). Structural complexity of simple Fe_2O_3 at high pressures and temperatures. *Nature Communications*, *7*(1), 10661.

[22] Zhu, H., Ma, Y., Yang, H., Ji, C., Hou, D., & Guo, L. (2010). Pressure induced phase transition of nanocrystalline and bulk maghemite (γ-Fe_2O_3) to hematite (α-Fe_2O_3). *Journal of Physics and Chemistry of Solids*, *71*(8), 1183-1186.

[23] Shanenkov, I., Sivkov, A., Ivashutenko, A., Medvedeva, T., & Shchetinin, I. (2019). High-energy plasma dynamic synthesis of multiphase iron oxides containing Fe_3O_4 and ε-Fe_2O_3 with possibility of controlling their phase composition. *Journal of Alloys and Compounds*, *774*, 637-645.

[24] Jaji, N. D., Lee, H. L., Hussin, M. H., Akil, H. M., Zakaria, M. R., & Othman, M. B. H. (2020). Advanced nickel nanoparticles technology: From synthesis to applications. *Nanotechnology Reviews*, *9*(1), 1456-1480.

[25] Mette, K., Kühl, S., Tarasov, A., Willinger, M. G., Kröhnert, J., Wrabetz, S., Trunschke, A., Scherzer, M., Girgsdies, F., Düdder, H., Kähler, K., Ortega, K. F., Muhler, M., Schlögl, R., Behrens, M., & Lunkenbein, T. (2016). High-temperature stable Ni nanoparticles for the dry reforming of methane. *ACS Catalysis*, *6*(10), 7238-7248.

[26] Mansur, H. S. (2010). Quantum dots and nanocomposites. *Wiley Interdisciplinary Reviews: Nanomedicine and Nanobiotechnology*, *2*(2), 113-129.

[27] Dahman, Y. (2017). *Nanotechnology and functional materials for engineers*. Elsevier.

[28] Yang, G. Z. (Ed.). (2018). *Implantable sensors and systems: From theory to practice*. Springer.

[29] Chen, H., Zhang, W., Li, M., He, G., & Guo, X. (2020). Interface engineering in organic field-effect transistors: Principles, applications, and perspectives. *Chemical Reviews*, *120*(5), 2879-2949.

[30] Avouris, P., Freitag, M., & Perebeinos, V. (2008). Carbon-nanotube photonics and optoelectronics. *Nature Photonics*, *2*(6), 341-350.

[31] Veetil, J. V., & Ye, K. (2009). Tailored carbon nanotubes for tissue engineering applications. *Biotechnology Progress*, *25*(3), 709-721.

[32] Zondlo, J. W. (2012). Graphite: Structure, properties, and applications. In *Graphite, graphene, and their polymer nanocomposites* (pp. 1-56). CRC Press.

[33] Wissler, M. (2006). Graphite and carbon powders for electrochemical applications. *Journal of Power Sources*, *156*(2), 142-150.

[34] Wen, J., Zhao, D., & Zhang, C. (2020). An overview of electricity powered vehicles: Lithium-ion battery energy storage density and energy conversion efficiency. *Renewable Energy*, *162*, 1629-1648.

[35] Di Lecce, D., Verrelli, R., & Hassoun, J. (2017). Lithium-ion batteries for sustainable energy storage: Recent advances towards new cell configurations. *Green Chemistry*, *19*(15), 3442-3467.

[36] Liu, Y., Shi, H., & Wu, Z. S. (2023). Recent status, key strategies and challenging perspectives of fast-charging graphite anodes for lithium-ion batteries. *Energy & Environmental Science*, *16*(11), 4834-4871.

[37] Asenbauer, J., Eisenmann, T., Kuenzel, M., Kazzazi, A., Chen, Z., & Bresser, D. (2020). The success story of graphite as a lithium-ion anode material--fundamentals, remaining challenges, and recent developments including silicon (oxide) composites. *Sustainable Energy & Fuels*, *4*(11), 5387-5416.

[38] Writer, B. (2019). Anode materials, SEI, carbon, graphite, conductivity, graphene, reversible, formation. In *Lithium-ion batteries* (pp. 1-71). Springer.

[39] Wen, Y., He, K., Zhu, Y., Han, F., Xu, Y., Matsuda, I., Ishii, Y., Cumings, J., & Wang, C. (2014). Expanded graphite as superior anode for sodium-ion batteries. *Nature Communications*, *5*(1), 4033.

[40] Anderson, O. L. (1984). A universal thermal equation-of-state. *Journal of Geodynamics*, *1*(2), 185-214.

[41] Ross, M., & Young, D. A. (1993). Theory of the equation of state at high pressure. *Annual Review of Physical Chemistry*, *44*(1), 61-87.

[42] Martin, J. J., & Hou, Y. C. (1955). Development of an equation of state for gases. *AIChE Journal*, *1*(2), 142-151.

[43] Canuto, V. (1975). Equation of state at ultrahigh densities. *Annual Review of Astronomy and Astrophysics*, *13*(1), 335-380.

[44] Menikoff, R. (2007). Empirical equations of state for solids. In *Shock wave science and technology reference library* (pp. 143-188). Springer.

[45] Martin, J. J. (1967). Equations of state—Applied thermodynamics symposium. *Industrial & Engineering Chemistry*, *59*(12), 34-52.

[46] Redlich, O., & Kwong, J. N. (1949). On the thermodynamics of solutions. V. An equation of state. Fugacities of gaseous solutions. *Chemical Reviews*, *44*(1), 233-244.

[47] Kontogeorgis, G. M., Liang, X., Arya, A., & Tsivintzelis, I. (2020). Equations of state in three centuries. Are we closer to arriving to a single model for all applications? *Chemical Engineering Science: X*, *7*, 100060.

[48] Bina, C. R., & Helffrich, G. R. (1992). Calculation of elastic properties from thermodynamic equation of state principles. *Annual Review of Earth and Planetary Sciences*, *20*(1), 527-552.

[49] Giovangigli, V., & Matuszewski, L. (2012). Supercritical fluid thermodynamics from equations of state. *Physica D: Nonlinear Phenomena*, *241*(6), 649-670.

[50] Tait, P. G. (1965). *Report on some of the physical properties of fresh water and of sea water*. Physics and Chemistry, *2*, 1-76.

[51] Birch, F. (1988). Elasticity and constitution of the Earth's interior. In *Elastic properties and equations of state* (Vol. 26, pp. 31-90). American Geophysical Union.

[52] Kholiya, K., & Chandra, J. (2014). Equation of state model for studying high-pressure compression behaviour of nanomaterials. *Journal of Taibah University for Science*, *8*(2), 137-141.

[53] Shanker, J., Kushwah, S. S., & Kumar, P. (1997). Theory of thermal expansivity and bulk modulus for MgO and other minerals at high temperatures. *Physica B: Condensed Matter*, *233*(1), 78-83.

[54] Sharma, S. M., Karmakar, S., Sikka, S. K., Teredesai, P. V., Sood, A. K., Govindaraj, A., & Rao, C. N. R. (2001). Pressure-induced phase transformation and structural

resilience of single-wall carbon nanotube bundles. *Physical Review B*, *63*(20), 205417.

[55] Venkateswaran, U. D., Rao, A. M., Richter, E., Menon, M., Rinzler, A., Smalley, R. E., & Eklund, P. C. (1999). Probing the single-wall carbon nanotube bundle: Raman scattering under high pressure. *Physical Review B*, *59*, 10928.

[56] Tang, J., Qin, L. C., Sasaki, T., Yudasaka, M., Matsushita, A., & Iijima, S. (2000). Compressibility and polygonization of single-walled carbon nanotubes under hydrostatic pressure. *Physical Review Letters*, *85*(9), 1887-1889.

[57] Hasegawa, M., & Nishidate, K. (2004). Radial deformation and stability of single-wall carbon nanotubes under hydrostatic pressure. *Physical Review B*, *70*(20), 205431.

[58] Elliott, J. A., Sandler, J. K. W., Windle, A. H., Young, R. J., & Shaffer, M. S. P. (2004). Collapse of single-wall carbon nanotubes is diameter dependent. *Physical Review Letters*, *92*(9), 095501.

[59] Chen, B., et al. (2002). Particle-size effect on the compressibility of nanocrystalline alumina. *Physical Review B*, *66*, 144101.

[60] Suryanarayana, C., & Koch, C. C. (2000). Nanocrystalline materials – Current research and future directions. *Hyperfine Interactions*, *130*(1-4), 5-44.

[61] Yakobson, B. I., Brabec, C. J., & Bernholc, J. (1996). Nanomechanics of carbon tubes: Instabilities beyond linear response. *Physical Review Letters*, *76*(14), 2511-2514.

[62] Ru, C. Q. (2000). Effective bending stiffness of carbon nanotubes. *Physical Review B*, *62*(15), 9973-9976.

[63] Lourie, O., & Wagner, H. D. (1998). Evaluation of Young's modulus of carbon nanotubes by micro-Raman spectroscopy. *Journal of Materials Research*, *13*(9), 2418-2422.

[64] Chang, T., & Gao, H. (2003). Size-dependent elastic properties of a single-walled carbon nanotube via a molecular mechanics model. *Journal of the Mechanics and Physics of Solids*, *51*(6), 1059-1074.

[65] Shen, L., & Li, J. (2004). Transversely isotropic elastic properties of single-walled carbon nanotubes. *Physical Review B*, *69*(4), 045414.